Fullerene mixing effect on carrier formation in bulk-hetero organic solar cell

doi: 10.1038/srep09483

SCIENTIFIC REPORTS

OPEN

SUBJECT AREAS:
SOLAR CELLS
LIGHT HARVESTING
POLYMERS

Received
17 November 2014

Accepted
6 March 2015

Published
30 March 2015

Correspondence and requests for materials should be addressed to Y.M. (moritomo.yutaka.gf@u.tsukuba.ac.jp)

Fullerene mixing effect on carrier formation in bulk-hetero organic solar cell

Yutaka Moritomo[1,2], Takeshi Yasuda[3], Kouhei Yonezawa[1], Takeaki Sakurai[1,4], Yasuo Takeichi[5], Hiroki Suga[6], Yoshio Takahashi[5,7], Nobuyuki Inami[5], Kazuhiko Mase[5] & Kanta Ono[5]

[1]Faculty of Pure and Applied Science, Univ. of Tsukuba, Tsukuba 305-8571, Japan, [2]Center for Integrated Research in Fundamental Science and Engineering (CiRfSE), Univ. of Tsukuba, Tsukuba 305-8571, Japan, [3]Photovoltaic Materials Unit, National Institute for Materials Science (NIMS), Tsukuba, Ibaraki 305-0047, Japan, [4]PRESTO, Japan Science and Technology Agency, Saitama 332-0012, Japan, [5]Institute of Materials Structure Science, High-Energy Accelerator Research Organization (KEK), Tsukuba, Ibaraki 305-0801, Japan, [6]Department of Earth and Planetary Systems Science, Hiroshima University, Higashi-hiroshima, Hiroshima 739-8526, Japan, [7]Department of Earth and Planetary Science, Univ. of Tokyo, Bunkyo-ku, Tokyo 113-0033, Japan.

Organic solar cells (OSCs) with a bulk-heterojunction (BHJ) are promising energy conversion devices, because they are flexible and environmental-friendly, and can be fabricated by low-cost roll-to-roll process. Here, we systematically investigated the interrelations between photovoltaic properties and the domain morphology of the active layer in OSCs based on films of poly-(9,9-dioctylfluorene-co-bithiophene) (F8T2)/[6,6]-phenyl C_{71}-butyric acid methyl ester ($PC_{71}BM$) blend annealed at various temperatures (T_{an}). The scanning transmission X-ray microscopy (STXM) revealed that fullerene mixing ($\Phi_{Fullerene}$) in the polymer matrix decreases with increase in T_{an} while the domain size (L) is nearly independent of T_{an}. The TEM-S mapping image suggests that the polymer matrix consist of polymer clusters of several nm and fullerene. We found that the charge formation efficiency (Φ_{CF}), internal quantum efficiency (Φ_{IQ}), and power conversion efficiency (PCE) are dominantly determined by $\Phi_{Fullerene}$. We interpreted these observations in terms of the polymer clusters within the polymer matrix.

In OSCs, the light-to-electric energy conversion is realized by the combination of the carrier formation and transfer processes within the active layer (Fig. S1). In the former process, the photo irradiation creates a donor exciton in the donor region and the donor exciton migrates to the donor (D)/acceptor (A) interface. Finally, the exciton separates into the electron and hole at the D/A interface. In most cases, the electron and hole are weakly bound to each other around the interface. In the latter process, the carriers transfer to the collector electrode and are collected as photocurrent. This is in a sharp contrast with an inorganic solar cell (ISC), in which the photo-irradiation directly creates carriers within the active layer.

The BHJ active layer of OSC consists of phase-separated nano-size (several tens of nm) domains of the donor polymer and acceptor fullerene[1–5]. The nano-size structure is essential for the efficient carrier formation process, because the length of exciton migration is ~3 nm. The STXM around the carbon K-edge is a powerful tool to clarify the molecular mixing as well as the domain structure in the BHJ active layer[6,7], because it can distinguish the fullerene carbon from the polymer carbon. For example, Collins *et al.*[6] revealed the fullerene mixing in the polymer matrix of PTB7/$PC_{71}BM$ blend film. Due to the low spatial resolution (~several tens of nm) of STXM, however, the domain size had to be enlarged by chemical admixture[6] or thermal annealing at higher temperature[7]. Recently, several experiments revealed sub-structures within the large domains. By means of atomic force microscopy (AFM) coupled with plasma-ashing technique, Hedley *et al.*[8] investigated sub-structure inside the domain (100–200 nm) of PTB7/$PC_{71}BM$ blend film prepared without additive and found that the domain consists of a large number of small fullerene spheres (20–60 nm). By means of energy-filtered electron transmission microscopy (EFTEM), Kesave *et al.*[9] reported fiber-like structure, ~10 nm wide and ~100 nm long, in PGeBTBT/$PC_{71}BM$ blend film.

On the other hands, the femtosecond time-resolved spectroscopy is a powerful tool to reveal the carrier formation process within the active layer[10–14], because the spectroscopy monitors the relative numbers of the photo-created exciton and carrier in the time domain. Significantly, the spectroscopy decouples the carrier formation and transfer processes, because the former process completes within several tens of ps. Actually, the time-resolved spectroscopy revealed that the exciton-to-carrier conversion process in PTB7/$PC_{71}BM$ blend film completes within ~0.3 ps[10].

In order to clarify the interrelation between molecular mixing and the photovoltaic properties of BHJ-type OSCs, we selected a liquid-crystalline semiconducting polymer, F8T2, as the donor polymer, because the domain

structure of the blend film with fullerene derivatives remains large (several hundreds of nm) and independent of T_{an}[15,16]. Yasuda *et al.*[16] systematically investigated the photovoltaic properties of the OSCs based on films of F8T2/$PC_{71}BM$ (33 : 67 wt. %) blend annealed at various temperature (T_{an}): the PCE systematically decreases from the optimal value (=2.28%) at T_{an} = 80°C to 0.81% at 240°C. Yonezawa *et al.*[17] investigated the charge formation dynamics of F8T2/$PC_{71}BM$ blend film by means of the femtosecond time-resolved spectroscopy. Here, we systematically investigated T_{an}-dependence of the photovoltaic properties, *i.e.*, short-circuit current (J_{sc}), open-circuit voltage (V_{oc}), fill factor (FF), power conversion efficiency (PCE), internal quantum efficiency (Φ_{IQ}), charge formation efficiency (Φ_{CF}), domain size (L), and fullerene mixing ($\Phi_{Fullerene}$,) in the polymer matrix in the OSCs based on films of F8T2/$PC_{71}BM$ blend. Φ_{CF} is defined by n_{formed}/n_{photon}, where n_{formed} and n_{photon} are the numbers of the carriers formed at the D/A interface (include weakly bound state) and the absorbed photons, respectively. Absolute value of n_{formed} was estimated by combination of the time-resolved and electrochemical spectroscopies. Φ_{CF} is the same as the exciton quenching efficiency, if all the quenched excitons are converted to carriers. We found that Φ_{CF}, Φ_{IQ}, and PCE are dominantly determined by $\Phi_{Fullerene}$, indicating an essential role of the fullerene mixing in the polymer matrix on the carrier formation and transfer processes.

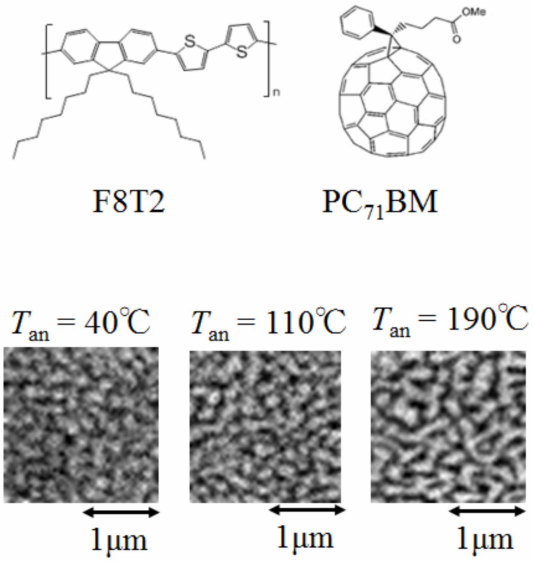

Figure 1 | STXM image of F8T2/$PC_{71}BM$ blend films at 284.4 eV. The bright regions correspond to the $PC_{71}BM$-rich domains, while the dark regions the F8T2-rich domains.

Results

Photovoltaic properties. First of all, let us survey the device parameter, *i.e.*, J_{sc}, V_{oc}, FF, PCE, and Φ_{IQ} against T_{an} (Table I). We fabricated OSCs based on films of F8T2/$PC_{71}BM$ (33 : 67 wt%) blend annealed for 10 min at T_{an} (Fig. S2). We measured current (J) – voltage (V) curve (Fig. S3) and incident photon-to-current conversion efficiency (IPCE) spectra (Fig. S4) .The magnitudes of J_{sc} and FF decrease with increase in T_{an}, while V_{oc} remains nearly independent of T_{an}. As a result, PCE ($=J_{sc} \times V_{oc} \times FF/I_0$, where I_0 is the power density of the incident light) deceases with increase in T_{an}. The T_{an}-dependence of J_{sc} and FF is ascribed to several compounded factors, *e.g.*, the domain size, carrier recombination process at the D/A interface, and connectivity among the domains. We confirmed that the domain size (L) of the active layered is nearly independent of T_{an} (*vide infra*).

Domain structure as investigated by STXM image. Figure 1 shows STXM images of the F8T2/$PC_{71}BM$ blend films annealed at various T_{an} probed at 284.4 eV. The photon energy (284.4 eV) was at the π*-resonance absorption of the fullerene framework[6,18]. Therefore, the bright regions correspond to the fullerene-rich domains, while the dark regions the polymer-rich domains. We performed two-dimensional Fourier transformation to evaluate the length scale (L) of the fullerene domain. We regarded the local maxima of the Fourier component as L (Fig. S5). We found that L (~270 nm) is nearly independent of T_{an}.

Fullerene mixing as investigated by STXM spectroscopy. To determine the fullerene mixing, we measured the carbon K-edge absorption spectra (ϕ_{exp}) at every 40 nm within the 2 μm × 2 μm image, *i.e.*, 50 × 50 spectra[19]. We should be careful for evaluation of the molecular mixing since the STXM spectra is average along the depth direction. We investigated cross-sectional Plasmon loss image (Fig. S6) of the blend film annealed at 80°C. We confirmed that the polymer matrix passes completely through to the other side. That is, the fullerene mixing of the polymer matrix is accurately evaluated by the STXM spectroscopy. Unfortunately, we cannot accurately evaluated the molecular mixing of the fullerene domain, because it overlaps with the polymer domain in the depth direction.

Upper panel of Fig. 2 shows the averaged carbon K-edge absorption spectra of the polymer matrix against T_{an}. We observed extra bands at both sides of the main peak at 285 eV, as indicated by downward arrows. The bands are ascribed to the 1st and 3rd peaks of $PC_{71}BM$ (see the lower panel of Fig. 2). Their intensities gradually increases with decreases in T_{an}, indicating that the fullerene mixing increases with decreases in T_{an}. The magnitudes of $\Phi_{Fullerene}$ were evaluated by least-squares fitting of the ϕ_{exp} spectra with the linear combination of the F8T2 (ϕ_D) and $PC_{71}BM$ (ϕ_A) spectra, $\phi_{cal} = C_D\phi_D + C_A\phi_A$. In the lower panel of Fig. 2, we show an example of the least-squares fitting. The linear combination (black thin curve) well reproduces the overall features of the ϕ_{exp} spectra. This indicates that the charge-transfer-type absorption at the D/A interface has negligible effects on the ϕ_{exp} spectra. In the spectral analysis, we select ten ϕ_{exp} spectra at every T_{an} at the central position of the polymer matrix to avoid the artificial mixing of the materials. The averages and standard deviations of C_D and C_A were evaluated. The $\Phi_{Fullerene}$ values were calculated by $C_A/(C_D + C_A)$, and are listed in Table II.

Carrier formation efficiency. We evaluate the absolute value of Φ_{CF} by combination of the femtosecond time-resolved and

Table I | Device parameters, *i.e.*, J_{sc}, V_{oc}, FF, PCE and Φ_{IQ} of OSCs based on films of F8T2/$PC_{71}BM$ (33 : 67 wt%) blend annealed for 10 min at T_{an}. The error bars of J_{sc}, V_{oc}, FF, PCE, and Φ_{IQ} were estimated from standard deviations of more than five OSC devices

T_{an} (°C)	J_{sc} (mA/cm²)	V_{oc} (V)	FF	PCE (%)	Φ_{IQ} @ 400 nm
40	4.37 ± 0.08	0.96 ± 0.01	0.516 ± 0.003	2.17 ± 0.04	0.368 ± 0.011
80	4.17 ± 0.08	0.97 ± 0.01	0.521 ± 0.003	2.12 ± 0.04	0.342 ± 0.009
110	3.96 ± 0.17	0.987 ± 0.006	0.486 ± 0.002	1.92 ± 0.09	0.336 ± 0.009
150	3.68 ± 0.19	0.94 ± 0.02	0.40 ± 0.01	1.37 ± 0.01	0.285 ± 0.007
190	3.51 ± 0.10	0.92 ± 0.01	0.387 ± 0.003	1.25 ± 0.05	0.300 ± 0.010
240	2.94 ± 0.17	0.91 ± 0.01	0.35 ± 0.01	0.95 ± 0.06	0.310 ± 0.015

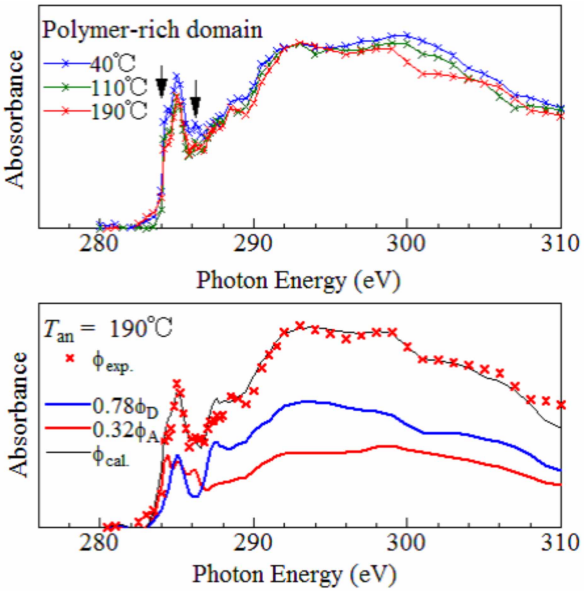

Figure 2 | Carbon K-edge absorption spectra of the polymer matrix. Upper panel shows the averaged absorption spectra against T_{an}. Lower panel shows an example of the spectral decomposition, which was performed by least-squares fitting of the observed spectra (ϕ_{exp}) with the linear combination of the F8T2 (ϕ_D) and $PC_{71}BM$ (ϕ_A) spectra, $\phi_{cal} = C_D\phi_D + C_A\phi_A$.

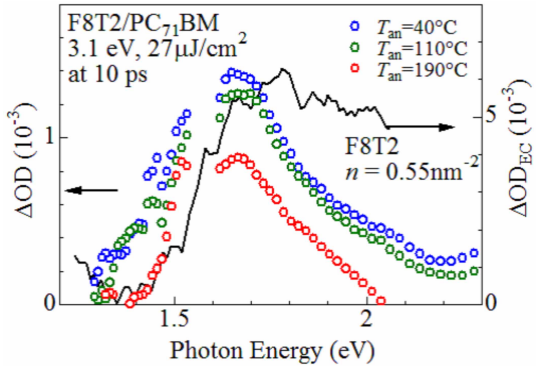

Figure 3 | Differential absorption (ΔOD) spectra at 10 ps of F8T2/$PC_{71}BM$ blend film and differential absorption (ΔOD_{EC}) spectrum of electrochemically oxidized F8T2 neat film. In ΔOD, the excitation photon energy and pulse energy are 3.1 eV and 27 μJ/cm^2, respectively. In ΔOD_{EC}, the hole-doing level (n) is 0.55 nm^{-2}.

electrochemical spectroscopies[20]. Solid curve in Fig. 3 is the differential absorption (ΔOD_{EC}) spectrum of electrochemically oxidized F8T2 neat film. The observed absorption at 1.8 eV is ascribed to the donor carrier. We investigated the spectral intensity ($I_{1.8eV}$) at 1.8 eV against the hole-doping level (n) and determined the coefficient ($\alpha_{carrier} = 4.1 \times 10^{-3}$ nm^2) between $I_{1.8eV}$ and n (see Fig. S7). Circles in Fig. 3 is the differential absorption (ΔOD) spectra at 10 ps of the F8T2/$PC_{71}BM$ blend film. A sharp photoinduced absorption (PIA) is observed at 1.7 eV, whose profile is similar to that of the ΔOD_{EC} spectrum. We confirmed that the spectral profile is unchanged after 10 ps. In addition, the decay time of the PIA is very long (=300 ps). These observations indicate that the PIA is due to the donor carriers. We evaluated the coefficient (α_{photon}) between the spectral intensity ($I_{1.7eV}$) at 1.7 eV and the number (n_{photon}) of the absorbed photons, with considering the reflection and transmission losses. The Φ_{CF} values were calculated by $\alpha_{photon}/\alpha_{carrier}$, and are listed in Table II.

Correlation between parameters. We summarize in Fig. 4 the interrelation among Φ_{CF}, $\Phi_{Fullerene}$, L, Φ_{IQ}, and PCE in OSCs against T_{an}. We note that Φ_{CF} has no relation with any losses after the carrier formation, *e.g.*, the carrier recombination at the D/A interface or carrier trapping. In this sense, Φ_{CF} is easier to interpret than the other efficiencies such as Φ_{IQ}, and PCE. Φ_{CF} systematically decreases from 0.78 to 0.48 with increase in T_{an}. In the 2nd and 3rd panels, we plotted $\Phi_{Fullerene}$ and L. The T_{an} value has no effect on the domain size ($L \sim 270$ nm), but seems to suppress $\Phi_{Fullerene}$ in the polymer matrix. The T_{an}-dependence of $\Phi_{Fullerene}$, however, is unclear due to rather large error bars. The error bars come from the bad signal/noise ratio in the featureless spectra. We carefully investigated T_{an}-dependence of the spectral profile around the fullerene peaks (284–287 eV) in the averaged carbon K-edge absorption spectra. We found that the relative intensities ($I_{284.4eV}$) of the fullerene peak at 284.4 eV systematically decreases with increase in T_{an} (Fig. S8). This observation indicates that the fullerene mixing in the polymer matrix decreases with increase in T_{an}. Thus observed T_{an}-dependence of the fullerene mixing is reasonable, because the thermal annealing at higher T_{an} accelerates the phase-separation into more pure domains. Our analysis revealed that the fullerene mixing in the polymer matrix is advantageous for the efficient carrier formation. The decrease in Φ_{CF} with T_{an} is responsible for the suppressed Φ_{IQ} and PCE (bottom panel of Fig. 4).

Discussion

To investigate the morphology within the polymer matrix, we investigated cross-sectional TEM-S mapping image of the blend film annealed at 80°C (Fig. S9). The mapping clarifies the distribution of the F8T2 polymer in ~ nm resolution. The mapping suggests that the F8T2 polymer matrix consists of the polymer clusters of several nm and the fullerene. Such a sub-structure well explains why the F8T2/$PC_{71}BM$ OSC shows high Φ_{IQ} (=0.35 at 40°C) even though

Table II | Internal quantum efficiency (Φ_{IQ}), carrier formation efficiency (Φ_{CF}), carrier transfer efficiency ($\Phi_{CT} = \Phi_{IQ}/\Phi_{CF}$), and fullerene mixing ($\Phi_{Fullerene}$) within the polymer matrix of OSCs based on films of F8T2/$PC_{71}BM$ (33 : 67 wt%) blend annealed for 10 min at T_{an}. The error bars of Φ_{CF} were roughly evaluated from the signal/noise ratio of the femtosecond time-resolved spectra. $\Phi_{Fullerene}$ was evaluated by least-squares fitting of the observed spectra (ϕ_{exp}) with the linear combination of the F8T2 (ϕ_D) and $PC_{71}BM$ (ϕ_A) spectra, $\phi_{cal} = C_D\phi_D + C_A\phi_A$. The averages and standard deviations of C_D and C_A were evaluated from ten ϕ_{exp} spectra at every T_{an}. The $\Phi_{Fullerene}$ values were calculated by $C_A/(C_D + C_A)$

T_{an} (°C)	Φ_{IQ} @ 400 nm	Φ_{CF} @ 400 nm	Φ_{CT} @ 400 nm	C_D	C_A	$\Phi_{Fullerene}$
40	0.368 ± 0.011	0.76 ± 0.04	0.48 ± 0.04	0.75 ± 0.07	0.47 ± 0.05	0.38 ± 0.08
80	0.342 ± 0.009	0.76 ± 0.04	0.45 ± 0.04	0.85 ± 0.05	0.36 ± 0.06	0.29 ± 0.08
110	0.336 ± 0.009	0.69 ± 0.04	0.49 ± 0.04	0.84 ± 0.04	0.36 ± 0.04	0.30 ± 0.05
150	0.285 ± 0.007	0.53 ± 0.04	0.53 ± 0.05	0.90 ± 0.07	0.33 ± 0.05	0.27 ± 0.07
190	0.300 ± 0.010	0.48 ± 0.04	0.63 ± 0.07	0.76 ± 0.03	0.31 ± 0.06	0.29 ± 0.09
240	0.310 ± 0.015	0.59 ± 0.04	0.53 ± 0.06	—	—	—

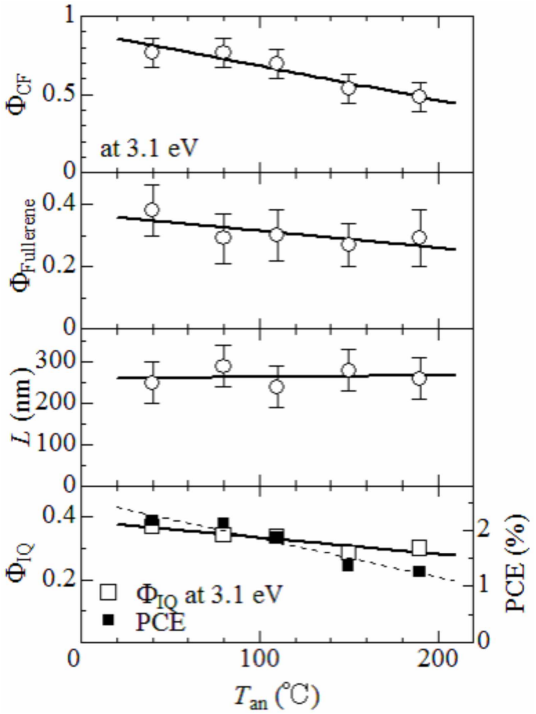

Figure 4 | Interrelation among Φ_{CF}, $\Phi_{Fullerene}$, L, Φ_{IQ}, and PCE in OSCs against T_{an}. Solid straight lines are the results of the lease-squares fittings. Error bars of Φ_{IQ}, and PCE are within the symbol size.

its domain size ($L \sim 270$ nm) is too large for exciton to reach the domain boundaries. According to this scenario, our observation, *i. e.*, Φ_{CF}, Φ_{IQ}, and PCE decreases as the fullerene mixing in the polymer matrix decreases, is interpreted as follows. With increase in T_{an}, the number (size) of the polymer clusters decreases (increases) within the polymer matrix, because the thermal annealing at higher T_{an} accelerates the phase-separation into more pure domains in every scale. As a result, the average fullerene concentration ($\Phi_{Fullerene}$) within the polymer matrix decreases with T_{an}. The decrease in number and the increase in size of the polymer clusters lead to less donor exciton reaching to the D/A interface, to cause the suppressed Φ_{CF}, Φ_{IQ}, and PCE. The fullerene mixing is a two-edged blade, because the sub-structure interface also function as recombination point for the photo-generated carriers[21]. Here, we define the carrier transfer efficiency (Φ_{CT}) as $n_{collected}/n_{formed}$, where $n_{collected}$ is the number of the carriers collected as photocurrent (Fig. S1). Then, Φ_{CT} is evaluated by Φ_{IQ}/Φ_{CT} (see Table II). We found that Φ_{CT} decreases with decrease in T_{an}. The suppressed Φ_{CT} is ascribed to the enhanced carrier recombination process at the sub-structure interface.

Summary

In summary, we systematically investigated the interrelations between photovoltaic properties, Φ_{CF}, and $\Phi_{Fullerene}$ in OSCs based on films of F8T2/$PC_{71}BM$ blend annealed at various T_{an}. We found that Φ_{CF}, Φ_{IQ}, and PCE are dominantly determined by $\Phi_{Fullerene}$, not by the size scale (L) of the domain. The TEM-S mapping image suggests that F8T2 polymer matrix consist of the polymer clusters of several nm and the fullerene. We interpreted the observation in terms of the polymer clusters within the polymer matrix: the decrease in number and the increase in size of polymer clusters lead to less donor exciton reaching to the D/A interface, to causes of the suppressed Φ_{CF}, Φ_{IQ}, and PCE. Even though the stability of the large-scale morphology against T_{an} is specific to the F8T2/$PC_{71}BM$ combination, the annealing effects on the sub-structure are considered to be general to the polymer/fullerene blend film. Thus, complementary study of STXM, which probes quantitative molecular mixing in several tens of nm scale, and TEM-S mapping, which probes molecular distribution in $\sim$ nm resolution, is effective to comprehend the photovoltaic properties of OSCs.

Method

Synthesis and characterization of the blend film. F8T2 was purchased from American Dye Source. The weight average molecular weight M_w, number average molecular weight M_n, and polydispersity M_w/M_n were estimated to be 45,000, 13,000, and 3.4, respectively. $PC_{71}BM$ (purity 99%) was purchased from Solenne.

For the STXM measurements, F8T2/$PC_{71}BM$ blend films were transferred to a Si_3N_4 membrane. A bilayer film [poly(sodium 4-styrenesulfonate) (PSS)/blend film] was prepared by successive spin-coating of an aqueous solution of PSS and an *o*-dichlorobenzene (*o*-DCB) solution of F8T2/$PC_{71}BM$ (33 : 67 wt %). The thicknesses of the as-grown films were 71 nm. The films were annealed for 10 min at T_{an} = 40, 80, 110, 150, 190, and 240°C in a N_2 glove box. Then, the bilayer film was cut into 1 × 1 mm^2 pieces, and the substrate was immersed for several minutes in distilled water to etch away the PSS film. Thus, we obtained small F8T2/$PC_{71}BM$ films floating on the distilled water. A piece of the floating film was scooped up with the Si_3N_4 membrane (50 nm in thickness and 500 × 500 μm^2 in area).

For the time-resolved spectroscopy, F8T2/$PC_{71}BM$ blend films were prepared by spin-coating of an *o*-DCB solution of F8T2/$PC_{71}BM$ (33 : 67 wt %) on quartz substrates. The thicknesses of the as-grown films were 60–70 nm. The films were annealed for 10 min at T_{an} = 40, 80, 110, 150, 190, and 240°C in a N_2 glove box. The atomic force microscope (AFM) image of the blend film annealed below 190°C revealed a periodic nanostructure of 300 nm in diameter (Fig. S2). The blend film annealed at 240°C is known to show macro-scale phase-separation into pure-F8T2 and pure-$PC_{71}BM$ domains.

Fabrication and characterization of the OSC. The OSCs were fabricated with a structure of indium tin oxide (ITO)/poly(3,4-ethylenedioxythiophene) (PEDOT):PSS (40 nm)/blend film/LiF (1 nm)/Al (80 nm). The patterned ITO (conductivity: 10 Ω/square) glass was pre-cleaned in an ultrasonic bath of acetone and ethanol and then treated in an ultraviolet-ozone chamber. A thin layer (40 nm) of PEDOT:PSS was spin-coated onto the ITO and dried in air at 110°C for 10 min on a hot plate. The substrate was then transferred to an N_2 glove box and dried again at 110°C for 10 min on a hot plate. An *o*-DCB solution of F8T2:$PC_{71}BM$ (33 : 67 wt %) was subsequently spin-coated onto the PEDOT:PSS surface to form the active layer. The resultant substrates were then annealed at T_{an} = 40, 80, 110, 150, 190, and 240°C for 10 min in a N_2 glove box. Finally, LiF (1 nm) and Al (80 nm) were deposited onto the active layer by conventional thermal evaporation at a chamber pressure lower than 5 × 10^{-4} Pa. The active area of the OSCs is 2 × 2 mm^2. The *J* - *V* curves (see Fig. S3) were measured using a voltage - current source/monitor under AM 1.5 solar-simulated light irradiation of 100 mW/cm^2 (Bunkou-keiki, OTENTO-SUN III). The IPCE spectra (see Fig. S4) was measured using a SM-250 system (Bunkou-keiki). The internal quantum efficiencies (Φ_{IQ}) at 400 nm were estimated with considering the reflection loss.

STXM spectroscopy and analysis. The STXM measurement was performed using the compact STXM installed at the BL-13A beamline of the Photon Factory (PF), KEK. The details of the compact STXM are described in the literature[19]. The spatial resolution was 30–40 nm. The carbon K-edge absorption spectra (ϕ_{exp}) were measured at every 40 nm within the 2 μm × 2 μm image, *i.e.*, 50 × 50 spectra. The molecular mixing was evaluated by least-squares fitting of the observed spectra (ϕ_{exp}) with the linear combination of the F8T2 (ϕ_D) and $PC_{71}BM$ (ϕ_A) spectra, $\phi_{cal} = C_D\phi_D + C_A\phi_A$. We regard the absorption spectra of the F8T2 and $PC_{71}BM$ domains in the F8T2/$PC_{71}BM$ blend film annealed at 240°C as ϕ_D and ϕ_A, respectively. The coefficients, C_A and C_D, are determined so that the evaluation function, $F(C_A,C_D) = \sum_i \phi_{exp}\left(\phi_{exp} - \phi_{cal}\right)^2$, becomes the minimum. The background constant component was subtracted so that ϕ_{cal} becomes zero at 280 eV. In the spectral analysis, we select the ten ϕ_{exp} spectra at the central position of the polymer matrix to avoid the artificial mixing of the materials. The averages and standard deviations of C_D and C_A were evaluated. The volume fractions of fullerene ($\Phi_{Fullerene}$) were calculated by $C_A/(C_D + C_A)$.

Femtosecond time-resolved spectroscopy. The time-resolved spectroscopy was performed in a pump-probe configuration. In order to reduce the irradiation damage, the blend films were placed in N_2 atmosphere. The pump pulse at 400 nm was generated as the second harmonics of a regenerative amplified Ti: sapphire laser in a β-BaB_2O_4 (BBO) crystal. The pulse width, repetition rate, and pulse energy were 100 fs, 1000 Hz, and 27 $\mu J/cm^2$ respectively. The frequency of the pump pulse was decreased by half (500 Hz) to provide "pump-on" and "pump-off" conditions. A white probe pulse (500–900 nm), generated by self-phase modulation in a sapphire plate was focused on the sample with the pump pulse. The spot sizes of the pump and probe pulses were 4.0 and 2.0 mm in diameter, respectively. The differential absorption (ΔOD) spectrum is expressed as $-\log(I_{on}/I_{off})$, where I_{on} and I_{off} are the transmission spectra under the pump-on and pump-off conditions, respectively.

Electrochemical spectroscopy. The electrochemical spectroscopy was carried out in an optical two-pole cell with a pair of quartz windows. The electrochemical hole-

doping was performed against Li metal in propylene carbonate (PC) solution containing 1 mol/L $LiClO_4$. The F8T2 neat film was spin-coated on an ITO glass substrate from *o*-DCB solution, and was dried in a N_2 glove box. The thicknesses was 67 nm. The active area of the film was 2.25 cm^2, and the reduction current was 100 nA. The voltage in the hole-doping process were 3.8 V vs. Li. The differential absorption (ΔOD_{EC}) spectrum of electrochemically oxidized film is expressed as $-\log(I_{doped}/I_{non})$, where I_{doped} and I_{non} are the transmission spectra of the hole-doped and non-doped films, respectively.

The charge formation efficiency (Φ_{CF}) was determined by combination of the time-resolved and electrochemical spectroscopies[20]. The former spectroscopy tells us the coefficient (α_{photon}) between ΔOD and n_{photon}, while the latter spectroscopy tells us the coefficient ($\alpha_{carrier}$) between ΔOD_{EC} and n. Then, the Φ_{CF} value is calculated by $\alpha_{photon}/\alpha_{carrier}$.

1. Hiramoto, M., Fujiwara, H. & Yokoyama, M. Three-layered organic solar cell with a photoactive interlayer of codeposited pigments. *Appl. Phys. Lett.* **58**, 1062–1064 (1991).
2. Sariciftci, N. S., Smilowitz, L., Heeger, A. J. & Wudl, F. Photoinduced electron transfer from a conducting polymer to buckminsterfullerene. *Science* **285**, 1474–1476 (1992).
3. Nguyen, T. L. *et al.* Semi-crystalline photovoltaic polymers with efficiency exceeding 9% in a ~300 nm thick conventional single-cell device. *Energy Environ. Sci.* **7**, 3040–3051 (2014).
4. Guo, X. *et al.* Enhanced photovoltaic performance by modulating surface composition in bulk heterojunction polymer solar cells based on PBDTTT-C-T/PC_{71} BM. *Adv. Mater.* **26**, 4043–4049 (2014).
5. He, Z. *et al.* Enhanced power-conversion efficiency in polymer solar cells using an inverted device structure. *Nature Photon.* **6**, 591–595 (2012).
6. Collins, B. A. *et al.* Absolute measurement of domain composition and nanoscale size distribution Explains Performance in PTB7:PC_{71}BM solar cells. *Adv. Energy Matter.* **3**, 65–74 (2013).
7. Ma, W. *et al.* Domain purity, miscibility, and molecular orientation at donor/acceptor interfaces in high performance organic solar cells: paths to further improvement. *Adv. Energy Mater.* **3**, 864–872 (2013).
8. Hedley, G. J. *et al.* Determining the optimum morphology in high-performance polymer-fullerene organic photovoltaic cells. *Nature Commun.* **4**, 2867 (2013).
9. Kesava, S. V. *et al.* Domain composition ad fullerene aggregation govern charge photogeneration in polymer/fullerene solar cells. *Adv. Energy Matter.* **4**, 1400116 (2014).
10. Yonezawa, K., Kamioka, H., Yasuda, T., Han, L. & Moritomo, Y. Fast carrier formation from acceptor exciton in low-gap organic photovotalic. *Appl. Phys. Express* **5**, 042302 (2012).
11. Guo, J. *et al.* Structure, dynamics, and power conversion efficiency correlations in a new Low bandgap polymer: PCBM solar cell. *J. Phys. Chem.* B **114**, 742–748 (2010).
12. Hwang, I.-W., Moses, D. & Heeger, A. J. Photoinduced carrier generation in P3HT/PCBM bulk heterojunction materials. *J. Phys. Chem. C* **112**, 4350–4354 (2008).
13. Guo, J., Ohkita, H., Benten, H. & Ito, S. Charge generation and recombination dynamics in Poly(3-hexylthiophene)/fullerene blend films with different regioregularities and morphologies. *J. Am. Chem. Soc.* **132**, 6154–6164 (2010).
14. Marsh, R. A., Hodgkiss, J. M., Albert-Seifried, S. & Friend, R. H. Effect of annealing on P3HT:PCBM charge transfer and nanoscale morphology probed by ultrafast spectroscopy. *Nano Lett.* **10**, 923–930 (2010).
15. Huang, J.-H. *et al.* Enhanced spectral response in polymer bulk heterojunction solar cells by using active materials with complementary spectra. *Sol. Energy Mater. Sol. Cells* **94**, 22–28 (2010).
16. Yasuda, T. *et al.* Photovoltaic properties and charge dynamics in nanophase-separated F8T2/PCBM blend films. *J. Photopolym. Sci. Technol.* **25**, 271–276 (2012).
17. Yonezawa, K. *et al.* Charge-transfer state and charge dynamics in poly (9,9′-dioctylfluorene-co-bithiophene) and [6, 6]-phenyl C_{70}-butyric acid methyl ester blend film. *Appl. Phys. Express* **4**, 122601 (2011).
18. Moritomo, Y. *et al.* Molecular mixing in donor and acceptor domains as investigated by scanning transmission X-ray microscopy. *Appl. Phys. Express* 7, 052302 (2014).
19. Takeichi, Y., Inami, N., Suga, H., Ono, K. & Takahashi, Y. Development of a compact scanning transmission X-ray microscope (STXM) at the photon factory. *Chem. Lett.* **43**, 373–375 (2014).
20. Moritomo, Y., Yonezawa, K. & Yasuda, T. Effect of temperature on carrier formation efficiency in organic photovoltaic cells. *Appl. Phys. Lett.* **105**, 073902 (2014).
21. Dimitov, S. D. & Durrant, J. R. Materials design consideration for charge generation in organic solar cells. *Chem. Mater.* **26**, 616–630 (2014).

Acknowledgments

This work was partially supported by a Grant-in-Aid (No. 23684022) for Scientific Research from the Ministry of Education, Culture, Sports, Science and Technology, Japan. The STXM measurements were performed under the approval of the Photon Factory Program Advisory Committee (Proposal No. 2013S2-003). We thank Dr. K. Yase of AIST for his helpful advice on the fabrication of the STXM samples.

Author contributions

Y.M. and T.Y. planed the overall the experiment. Y.M. analyzed the STXM spectra and wrote the main manuscript. T.Y. fabricated and characterized the organic solar cells. K.Y. performed time-resolved and experiment spectroscopies and their analyses. T.S. contribute the analyses of the X-ray absorption spectra. Y.T., H.S., Y.T., N.I., K.M. and K.O. construct and operated the STXM machine.

Additional information

Supplementary information accompanies this paper at http://www.nature.com/scientificreports

Competing financial interests: The authors declare no competing financial interests.

How to cite this article: Moritomo, Y. *et al.* Fullerene mixing effect on carrier formation in bulk-hetero organic solar cell. *Sci. Rep.* **5**, 9483; DOI:10.1038/srep09483 (2015).